Complex dynamics under tension in a high-efficiency frameshift stimulatory structure

Matthew T. J. Halma[a], Dustin B. Ritchie[a], Tonia R. Cappellano[a], Krishna Neupane[a], and Michael T. Woodside[a,1]

[a]Department of Physics, University of Alberta, Edmonton, AB, Canada T6G2E1

Edited by Marina V. Rodnina, Max Planck Institute for Biophysical Chemistry, Goettingen, Germany, and accepted by Editorial Board Member Yale E. Goldman July 15, 2019 (received for review March 27, 2019)

Specific structures in mRNA can stimulate programmed ribosomal frameshifting (PRF). PRF efficiency can vary enormously between different stimulatory structures, but the features that lead to efficient PRF stimulation remain uncertain. To address this question, we studied the structural dynamics of the frameshift signal from West Nile virus (WNV), which stimulates −1 PRF at very high levels and has been proposed to form several different structures, including mutually incompatible pseudoknots and a double hairpin. Using optical tweezers to apply tension to single mRNA molecules, mimicking the tension applied by the ribosome during PRF, we found that the WNV frameshift signal formed an unusually large number of different metastable structures, including all of those previously proposed. From force-extension curve measurements, we mapped 2 mutually exclusive pathways for the folding, each encompassing multiple intermediates. We identified the intermediates in each pathway from length changes and the effects of antisense oligomers blocking formation of specific contacts. Intriguingly, the number of transitions between the different conformers of the WNV frameshift signal was maximal in the range of forces applied by the ribosome during −1 PRF. Furthermore, the occupancy of the pseudoknotted conformations was far too low for static pseudoknots to account for the high levels of −1 PRF. These results support the hypothesis that conformational heterogeneity plays a key role in frameshifting and suggest that transitions between different conformers under tension are linked to efficient PRF stimulation.

programmed ribosomal frameshifting | RNA folding | pseudoknots | force spectroscopy | West Nile virus

Programmed ribosomal frameshifting (PRF) involves a recoding of the translation of mRNA by ribosomes owing to a shift in the reading frame, resulting in the production of an alternate polypeptide chain (1–4). PRF is triggered by a stimulatory structure in the mRNA, most often a pseudoknot formed when nucleotides within a hairpin loop base pair with complementary ones outside of the loop (5), in conjunction with a slippery sequence located 6 to 8 nt upstream, where the shift in reading frame takes place (2, 3, 6). PRF is particularly notable in viruses (7), many of which use a programmed shift into the −1 frame (−1 PRF) to produce 2 different polypeptides in a defined ratio. The expression ratio of the frameshifted proteins can affect essential aspects of viral function, such as genome replication and packaging or viral invasiveness (8–13), making it an attractive target for drugs aiming to attenuate viruses by altering PRF efficiency levels (14, 15).

The level of −1 PRF stimulated by different structures can vary enormously, from a few percent up to ∼70% to 80% (16–21). However, the features that contribute to efficient stimulation remain under debate (2), in part because the mechanisms driving frameshifting remain incompletely understood. Given that tension in the mRNA applied by the ribosome during translocation (22, 23) is a key feature of several proposed frameshifting mechanisms (2, 24, 25), it has been suggested that PRF efficiency is linked to the mechanical properties of the stimulatory structure (17, 24, 26). This hypothesis has motivated studies of stimulatory structures under mechanical tension using single-molecule force spectroscopy (SMFS), a powerful tool for studying conformational dynamics whereby force is applied to the ends of a molecule by a probe, such as optical tweezers, and the molecular extension is monitored as the structure changes in response to the tension (27). Such measurements applying force across the stimulatory structure can be used to mimic the tension applied by the translocating ribosome (22, 23) and characterize tension-induced dynamics in the stimulatory structure.

SMFS studies have uncovered interesting trends in the mechanical properties of frameshift stimulatory structures. Work examining pseudoknots containing mutations abolishing key tertiary contacts has suggested a correlation between PRF efficiency and the unfolding force for stimulatory pseudoknots (28, 29). However, a survey of numerous different pseudoknots showed that the mechanical resistance was uncorrelated to −1 PRF efficiency; instead, −1 PRF efficiency was found to correlate with conformational plasticity or heterogeneity (16). This correlation was supported by subsequent work extending SMFS studies of −1 PRF to other pseudoknots (30), different types of stimulatory structures such as hairpins (31), and the effects of antiframeshifting ligands (32). Evidence supporting the importance of conformational plasticity has also been found from single-molecule fluorescence experiments of ribosomes translocating through pseudoknots (33) and ensemble structural studies of stimulatory structures using such methods as selective 2′-hydroxyl acylation analyzed by primer extension (SHAPE) (21, 34). However, structures stimulating extremely high levels of frameshifting, which should pose the most stringent test of any hypotheses relating stimulatory structure properties and −1 PRF efficiency, have not yet been studied to probe their mechanical properties or dynamics.

Significance

Programmed ribosomal frameshifting (PRF) is important to many viruses, but how structures in mRNA stimulate PRF remains uncertain. By studying a frameshift signal stimulating very high PRF in West Nile virus (WNV), we identify features that differ from other structures stimulating more modest PRF levels. Using single-molecule force spectroscopy to mimic the effects of tension applied to the RNA by the ribosome during translation, we find that the WNV frameshift signal exhibits exceptionally heterogeneous conformational dynamics, forming several different pseudoknots and multiple combinations of hairpins, all connected on 2 mutually exclusive pathways. This work supports a role for conformational heterogeneity in PRF, suggesting that dynamic fluctuations rather than static properties play a key role in stimulating PRF efficiently.

Author contributions: D.B.R. and M.T.W. designed research; M.T.J.H., D.B.R., and K.N. performed research; M.T.J.H., D.B.R., and T.R.C. contributed new reagents/analytic tools; M.T.J.H. analyzed data; and M.T.J.H. and M.T.W. wrote the paper.

The authors declare no conflict of interest.

This article is a PNAS Direct Submission. M.V.R. is a guest editor invited by the Editorial Board.

See Commentary on page 19225.

[1]To whom correspondence may be addressed. Email: michael.woodside@ualberta.ca.

This article contains supporting information online at www.pnas.org/lookup/suppl/doi:10.1073/pnas.1905258116/-/DCSupplemental.

First published August 13, 2019.

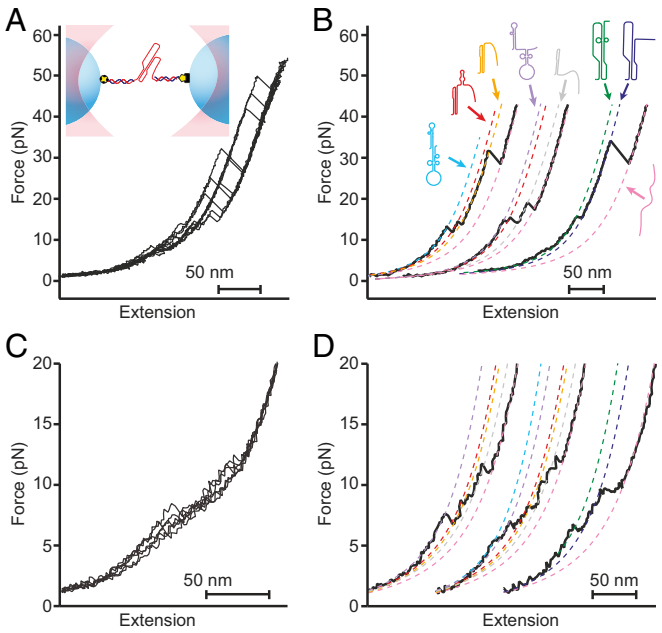

Fig. 1. Force spectroscopy measurements of the WNV frameshift signal. (*A*) Representative unfolding FECs from the same molecule showing multiple "rips" where the extension increases when different parts of the structure unfold as the force is ramped up. (*Inset*) The frameshift signal is held under tension via duplex handles connected to beads held in optical traps. (*B*) Fitting unfolding FECs (black) to WLC models containing different amounts of unfolded RNA (dashed lines) reveals multiple different conformations of the frameshift signal. Cartoons show proposed structures for the different states based on observed length changes and unfolding forces. (*C*) Representative refolding FECs showing heterogeneous behavior as in unfolding curves. (*D*) WLC fits (dashed lines) to refolding curves (black) reveal the same set of states (color-coded as in *B*) as seen in unfolding curves.

Here we report SMFS measurements of the frameshift signal from West Nile virus (WNV), a mosquito-borne flavivirus causing neurologic disease that uses −1 PRF to control the relative expression levels of structural and nonstructural proteins encoded within a single open reading frame (9). Whereas most viral frameshift signals stimulate −1 PRF with an efficiency in the range of 5% to 30% (16, 17), the WNV frameshift signal has been reported to do so at up to 70% efficiency (21), among the highest levels measured to date. The WNV frameshift signal is also notable because the nature of the stimulatory structure is unclear. Initial studies of a 75-nt segment of the WNV mRNA suggested that, based on bioinformatic predictions, the stimulatory structure is a 61-nt pseudoknot (35). However, subsequent work extending the RNA by ∼50 nt and applying SHAPE analysis suggested that the frameshift signal forms competing tandem stem loop and 109-nt pseudoknot structures (21), with the tandem stem loops sharing stem 1 in common with the 61-nt pseudoknot proposed previously but the 109-nt pseudoknot being mutually exclusive with the other structures.

Using optical tweezers to measure the unfolding and refolding of individual mRNA molecules held under tension, we aimed not only to test the link between −1 PRF stimulation efficiency and conformational heterogeneity in the case of an extremely efficient frameshift signal, but also to confirm which, if any, of the structures proposed for the WNV frameshift signal were formed. We found that the conformational dynamics of the WNV frameshift signal were much more complex than those of structures stimulating −1 PRF less efficiently, confirming the hypothesis. Indeed, the WNV frameshift signal formed all the structures proposed previously, as well as several others: analysis of the unfolding and refolding trajectories revealed 2 parallel pathways, each containing multiple intermediates. Suggestively, the number of transitions between these states was highest in the range of forces expected to be applied by the ribosome during −1 PRF, supporting the notion that dynamic conformational changes under tension rather than static properties play a key role in stimulating −1 PRF efficiently.

Results

We studied the 111 nucleotides downstream of the WNV slippery sequence and linker (*SI Appendix*, Table S1). We first used a dual-luciferase assay of frameshifting to confirm that this frameshift signal stimulated very high −1 PRF levels, finding a stimulation efficiency of 78 ± 8% (all errors represent standard error of the mean, SEM). For SMFS measurements, we next transcribed a RNA construct containing these 111 nucleotides flanked on each side by kilobase-long handle sequences, annealing the transcripts to single-stranded DNA complementary to the handle regions and attached to beads held in optical traps (Fig. 1 *A*, *Inset*) (16). The tethered RNA was held near zero force for 3 s to allow time for folding, after which the traps were separated at constant speed to ramp up the force before bringing them together to ramp the force back down. These force ramps mimicked the situation during −1 PRF, where the ribosome makes repeated attempts to resolve the stimulatory structure before finally translocating through it (33, 36), causing rapid, nonequilibrium fluctuations in tension in the mRNA.

Changes in structure were monitored by plotting the force as a function of the molecular extension, generating force-extension curves (FECs). FECs characteristically displayed regions in which the force rose nonlinearly with extension, reflecting the stretching of the handles during parts of the unfolding trajectory where the structure remained constant, separated by "rips" in the curve where the extension increased abruptly and the force dropped, indicating the unfolding of some part of the RNA (Fig. 1*A*). Notably, repeated unfolding of the same molecule revealed different patterns of rips of different length in the FECs (Fig. 1 *A* and *B*, black), indicating the presence of a heterogeneous mixture of conformational states. Similarly heterogeneous behavior was also seen in refolding curves (Fig. 1 *C* and *D*, black).

We characterized the structural transitions occurring in these FECs by fitting the curves to worm-like chain (WLC) polymer-elasticity models (37) before and after each rip (Fig. 1 *B* and *D*, dashed lines). Using one WLC for the duplex handles in series with a second WLC for the variable amount of unfolded RNA present in each conformation, we determined the contour length of unfolded RNA, L_c^U, before and after each transition. We identified at least 6 conformational states with different L_c^U values (Table 1), indicating a minimum of 6 different structures in the frameshift signal. Some of these states (Fig. 1*B*, orange and dark blue) unfolded with the broad distribution of generally high forces characteristic of tertiary structures such as pseudoknots (16, 38), whereas the others unfolded with a narrower distribution of forces in the range of 10 to 20 pN, more characteristic of simple duplexes (39, 40), suggesting the presence of 2 distinct kinds of pseudoknots as well as various helix and/or hairpin structures. The same set of L_c^U values from the WLC

Table 1. Unfolding lengths and forces of observed and predicted structures

Observed L_c^U, nm	Proposed state	Expected L_c^U, nm	Observed F_U, pN
0	DHP	0	10.8 ± 0.3
9 ± 1	DHP−	10.0	12.0 ± 0.3
	PK_D	9.8	11.4 ± 0.2
12.1 ± 0.8	PK_D−	12.4	21 ± 1
20.4 ± 0.6	PK_A+HP	20.5	13.0 ± 0.4
31 ± 1	PK_A	31.5	24 ± 1
40 ± 1	$S1_A$	40.9	16.7 ± 0.2
60.7 ± 0.4	U	61.3	

Errors represent SEM.

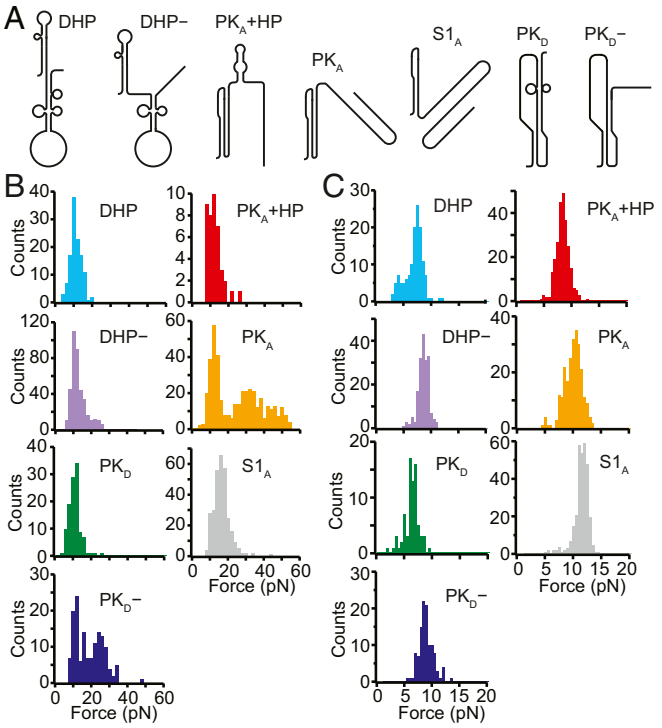

Fig. 2. Different structures formed by the WNV frameshift signal in FECs. (*A*) Secondary structure models for the different conformations matching the states observed in the FECs (see also *SI Appendix*, Fig. S1). (*B*) Unfolding force distributions for the different states. The unfolding forces for DHP, DHP−, S1$_A$, PK$_D$, and PK$_A$+HP were in the range of ∼5 to 20 pN, characteristic of secondary structures. (For PK$_D$, and PK$_A$+HP, a duplex/hairpin unfolded rather than the more stable pseudoknot.) Most unfolding forces for PK$_A$ and PK$_D$− were in the range of 20 to 60 pN, characteristic of fully formed pseudoknots, although some transitions occurred at lower force, suggesting incomplete tertiary contact formation. (*C*) Refolding force distributions for each state. Refolding forces were only slightly smaller than unfolding forces for DHP, DHP−, S1$_A$, PK$_D$, and PK$_A$+HP but were considerably smaller for PK$_A$ and PK$_D$−.

fits were seen for refolding as for unfolding (*SI Appendix*, Table S2), indicating that the same set of intermediate structures was sampled.

To identify the structures corresponding to each state in the FECs, we matched the observed L_c^U values to the expectations for the pseudoknot structures proposed in the literature as well as to the stem-loop structures predicted by *mfold* (41). Seven structures were found to match the observed L_c^U values within experimental error (Fig. 2*A* and *SI Appendix*, Fig. S1): the pseudoknot proposed by Firth and Atkins (35), denoted by PK$_A$, which unfolded over a broad range of forces (Fig. 2*B*, orange); a pseudoknot similar to that proposed by Moomau et al. (21), denoted by PK$_D$, which unfolded partially at low force (Fig. 2*B*, green); a partially folded version of PK$_D$, denoted by PK$_D$−, which unfolded over a broad range of forces (Fig. 2*B*, blue); fully and partially folded versions of the double-hairpin also proposed by Moomau et al. (21), denoted by DHP and DHP−, unfolding over a narrow range of low forces (Fig. 2*B*, cyan and purple, respectively); a combination of PK$_A$ and a short hairpin, denoted by PK$_A$+HP, unfolding partially over a narrow range of low forces (Fig. 2*B*, red); and an extended version of stem 1 from PK$_A$, denoted by S1$_A$, similar to one of the hairpins in DHP, which unfolded over a narrow range of low forces (Fig. 2B, gray). The correspondence of each structure to the observed lengths and unfolding forces is shown in Table 1.

These unfolding forces matched the expectation that tertiary structure unfolding generally involves broader force distributions and higher forces than secondary structure unfolding (16, 39). The sole exception was PK$_D$, whose unusually low unfolding force reflected the low-stability contacts at the 3′ end of stem 2, as revealed in SHAPE data (21). The forces observed in refolding were generally lower than the unfolding forces for the corresponding structures (Fig. 2*C*), with small differences for states where only secondary structure was broken/formed during unfolding/refolding (DHP, DHP−, S1$_A$, PK$_D$, PK$_A$+HP) but larger differences in the cases of PK$_D$− and PK$_A$, which involved breaking/forming tertiary structures. Thus, transitions involving secondary structures alone were not far from equilibrium, leading to the observation of occasional quasi-equilibrium reversible hopping between states (*SI Appendix*, Fig. S2), whereas those involving tertiary interactions were generally farther from equilibrium, as expected based on previous work (38, 42–44).

To confirm the structural assignments for these states, we remeasured the FECs in the presence of antisense oligonucleotides (*SI Appendix*, Table S1) binding to specific regions of the sequence at which they block RNA base pair formation (Fig. 3*A*, shaded regions). Considering first the oligo that blocked formation of stem 2 in both PK$_A$ and PK$_D$ (Fig. 3*A* and *SI Appendix*, Fig. S1, green), denoted by oligo 1, we found that unfolding events had forces in the range of 10 to 20 pN (Fig. 3*B*). This result indicates that only secondary structures were present, confirming that oligo 1

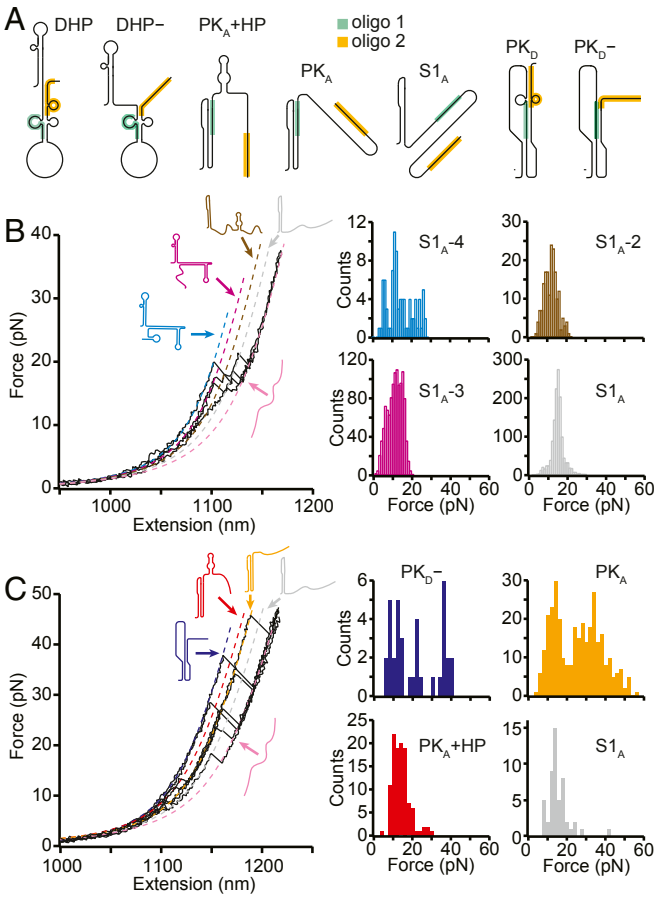

Fig. 3. FECs with antisense oligos. (*A*) Structural models showing where antisense oligos 1 (green) and 2 (orange) bind on each state. (*B*) With oligo 1 present, FECs showed only the low unfolding forces characteristic of secondary structures, indicating that the pseudoknots were prevented from forming, as expected from the structural models in *A*. Several unfolding transitions not observed without the oligo were seen, matching predictions for structures formed under the constraints imposed by the antisense oligo. (*C*) With oligo 2 present, high-force unfolding events corresponding to PK$_A$ and PK$_D$− were observed, but transitions corresponding to DHP and DHP− were not, consistent with the structural models in *A*.

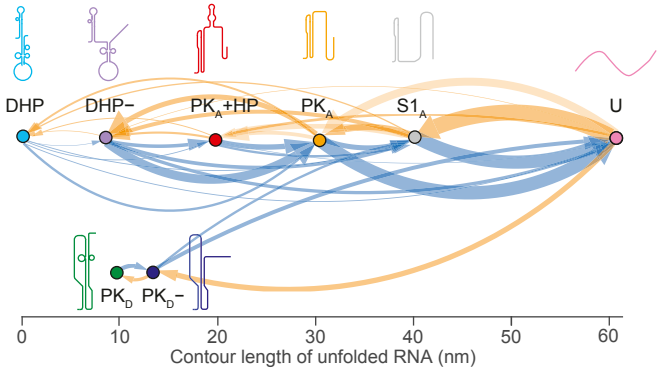

Fig. 4. Transition map of unfolding and refolding pathways. All pairwise transitions between states observed in unfolding (blue) and refolding (orange) FECs are shown, with the thickness of each arrow proportional to the probability of observing the associated transition. The same 2 distinct pathways are seen for both unfolding and refolding.

blocked pseudoknot formation. Indeed, not only were PK_A, PK_D, and PK_D− prevented from forming, but, based on the L_c^U values from WLC fits (Fig. 3*A*, dashed lines) to the different states observed in these FECs (*SI Appendix*, Table S3), so were all the other states in Fig. 2*A* with the exception of $S1_A$. In their stead, various combinations of $S1_A$ with nonnative helices that are energetically disfavored in the absence of antisense oligomer binding (*SI Appendix*, Fig. S3) were observed, matching predictions from structure-prediction tools (41, 45, 46).

A second antisense oligonucleotide (oligo 2) was used to block base-pairing at the 3′ end of the frameshift signal (Fig. 3*A* and *SI Appendix*, Fig. S1, orange), disrupting DHP, DHP−, and PK_D while permitting the formation of PK_A, PK_A+HP, PK_D−, and $S1_A$. High-force unfolding events were indeed seen with oligo 2 present, corresponding to unfolding of PK_A and PK_D− (Fig. 3*B*, orange and dark blue, respectively), as were lower-force events corresponding mainly to unfolding of PK_A+HP and $S1_A$ (Fig. 3*B*, red and gray, respectively). The contour lengths for unfolding these states matched the values observed without oligos and those expected from the structural models of each state (*SI Appendix*, Table S3) in all cases but one: PK_D−, which was slightly shorter (~1.5 nm) than without oligo 2. This difference is attributed to the fact that oligo 2 can invade stem 2 of PK_D− by 2 nt, shortening the expected length change on unfolding by 1.3 nm. States with the L_c^U and unfolding force values expected for DHP, DHP−, and PK_D were not observed in the presence of oligo 2, as expected; PK_D− was present, but its occupancy was reduced by roughly 2-fold.

Finally, we examined the sequence in which the states formed, cataloging all pairwise transitions between states during unfolding and refolding curves to reveal all possible pathways through them (47). The resulting transition maps for unfolding (Fig. 4, blue) and refolding (Fig. 4, orange) show 2 distinct pathways for both unfolding and refolding the WNV frameshift signal. Most unfolding and refolding FECs (80 ± 2% of each) involved transitions along a pathway involving $S1_A$, PK_A, and DHP (Fig. 4, *Top*), whereas a minority (20 ± 2%) were on a second pathway involving PK_D and PK_D− (Fig. 4, *Bottom*). The observed transitions on the 2 pathways were consistent with the properties of the structures identified for each state: on the most common pathway, DHP, DHP−, PK_A, and $S1_A$ all share a similar stem structure ($S1_A$) and thus can be interconverted readily, whereas the pseudoknots on the minority pathway have a stem structure inconsistent with DHP or PK_A and thus cannot interconvert with the latter structures. Note that even though PK_D and DHP− had similar unfolding forces and contour lengths, PK_D unfolded only via PK_D−, which could be readily identified by its distinctive L_c^U value and unfolding force (Table 1).

To complement the transition maps, we also analyzed how the occupancy of each state changed as a function of force during unfolding (Fig. 5*A*) and refolding (Fig. 5*B*). All the different structures that could be formed by the WNV frameshift signal were occupied at low force, with the exception of $S1_A$: roughly 16% of unfolding curves started in DHP, 50% started in DHP−, 9% started in PK_A+HP, 4% started in PK_A, 13% started in PK_D, and 8% started in PK_D−. The occupancies were similar when examining only the first pulls for each molecule (*SI Appendix*, Table S4), where the RNA had folded before it was tethered to the beads, suggesting that the distribution of states was not significantly affected by waiting only 3 s between successive pulls, and, moreover, that refolding under tension when tethered to beads was not significantly different from folding in the absence of force before tethering. However, the occupancies of PK_A and PK_A+HP were considerably higher at the end of refolding FECs than at the start of unfolding FECs, and the occupancy of DHP− was correspondingly lower (*SI Appendix*, Table S4), indicating that a significant reconfiguration of PK_A into the double-hairpin structures occurred between pulls. The low occupancy of DHP compared with DHP− could reflect the presence of transitions into DHP occurring at forces sufficiently low so as to preclude their ready identification; attempts to detect such transitions using an analysis sensitive to low-force transitions (48) were unsuccessful.

Discussion

Comparing the behavior of the WNV stimulatory structure with that of structures stimulating −1 PRF at more moderate levels, the most obvious difference is the extreme conformational plasticity of the WNV frameshift signal. Previous SMFS studies of stimulatory structures inducing −1 PRF with efficiencies in the range of 15% to 20%, like those from the severe acute respiratory syndrome coronavirus, sugar cane yellow leaf virus, and mouse mammary tumor virus (19, 20, 49), found that in each case, only 2 structures formed: the native pseudoknot and an alternate structure (16). In contrast, the WNV frameshift signal formed 3 different pseudoknot structures based on 2 mutually incompatible configurations, as well as several different stem-loop structures. Consequently, the folding of this RNA is remarkably complex, involving 2 largely disjunct pathways, each with multiple intermediate states. In fact, the SMFS measurements likely understate the full complexity of the pathways: H-type pseudoknots such as PK_A, PK_D, and PK_D− are known to have at least 2 parallel pathways involving stem 1 or stem 2 as intermediates, with the flux between the pathways determined by the relative stability of the 2 stems (50). However, the unfolding force of pseudoknots is often sufficiently high so as to make hairpin intermediates very short-lived and thus not always observed, as here; only the stem 1 intermediate ($S1_A$) of PK_A was seen, and none of the hairpin intermediates for PK_D or PK_D− were observed.

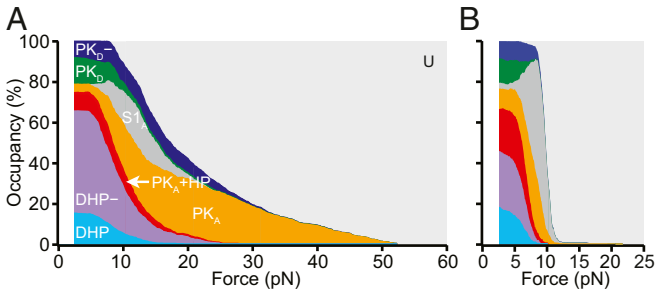

Fig. 5. Force-dependent conformational heterogeneity. The occupancy of the different conformations as a function of the force applied during unfolding (*A*) and refolding (*B*) highlights the extreme conformational heterogeneity of the WNV frameshift sequence. Differences between unfolding and refolding reflect the nonequilibrium nature of the transitions.

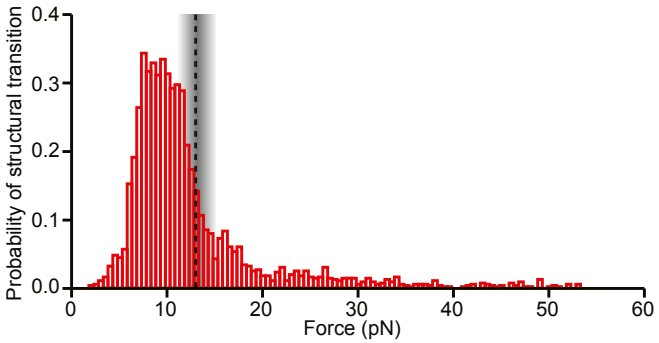

Fig. 6. Force-dependent probability of structural transitions. The probability of the WNV stimulatory structure changing conformation under tension during unfolding and refolding pulls peaks at ~7 to 13 pN, just below the maximum force applied by the ribosome during translocation before it stalls (dashed line).

The pathways defined in Fig. 4 have some interesting properties. From the transition maps, although the refolding pathways are completely disjunct, the unfolding pathways appear to be connected through $S1_A$: PK_D- never transitioned to PK_A, but it did sometimes appear to change directly into $S1_A$. In principle, such a change should not be seen, because $S1_A$ is incompatible with both stems in PK_D-. However, in every case, these transitions occurred in the same force range at which $S1_A$ refolds (~10 to 14 pN) (Fig. 2*C*, gray), so that $S1_A$ would be expected to form quite rapidly after unfolding of PK_D-, resulting in an apparent transition between PK_D- and $S1_A$. A more intriguing observation is that in the pathway starting at DHP, PK_A was able to form after the double-hairpin conformations unfolded, requiring the formation of new tertiary contacts during unfolding. This behavior is contrary to the standard hierarchy of events seen during unfolding, where typically tertiary structures unfold before secondary structures (38, 42–44), as seen in the pathway involving PK_D. However, such a conversion of a double hairpin to a pseudoknot has been reported previously in SMFS measurements of the *rpsO* operator from *Escherichia coli* (51); here it is enabled by the similarity between the refolding force for PK_A (Fig. 2*C*, orange) and the unfolding forces for DHP and DHP– (Fig. 2*B*, cyan and purple). The existence of direct transitions from the double hairpin to PK_A suggests that unfolding of the 3′ hairpin in DHP– is likely coordinated cooperatively with stem 2 formation in PK_A.

Turning to the various states observed by SMFS, the length changes and sequential transitions identified from the FECs help refine and expand on the results from previous studies of the WNV frameshift signal. The apparently incompatible structures proposed on the basis of bioinformatic predictions (35) and SHAPE analysis (21) were in fact all present, with their incompatibility resolved by their existence on separate, mutually exclusive pathways. The structure of the pseudoknot proposed by Moomau et al. (21) was refined based on the observed length changes, revealing 2 variants: one with a long stem 2 and the other with a truncated stem 2 (Fig. 2*A* and *SI Appendix*, Fig. S1). An additional variant of the double hairpin proposed by Moomau et al. (21) (DHP) was also observed, with one stem, DHP–, partially unfolded. Moreover, the unfolding force distributions for PK_A and PK_D- (Fig. 2*B*, orange and blue) suggested the presence of 2 populations: one without properly formed tertiary contacts that unfolded in the ~10 to 15 pN range characteristic of secondary structures and the other with a broader unfolding force distribution in the 20 to 50 pN range characteristic of pseudoknots with a fully formed tertiary structure. Importantly, all these structures were sufficiently stable (or metastable) so as to persist during the 3-s waiting period between successive FECs, such that significant fractions of the unfolding FECs started out in them.

The occupancies of the diverse conformational states formed by the WNV frameshift signal were not static, however: a considerable number of transitions between structures were observed under tension, including both quasi-equilibrium fluctuations between conformations and nonequilibrium switches from one structure to another. Looking at the probability of undergoing some form of structural transition in the FECs as a function of force (Fig. 6), we found that it was highly peaked in the range of 7 to 13 pN. Intriguingly and suggestively, this maximum is in the range of forces just below the force at which ribosomes have been observed to stall during translation, 13 ± 2 pN (52). Given that the ribosome ramps the force on the stimulatory structure up and down in multiple attempts to unfold it during −1 PRF (33, 36), at loading rates estimated to be even higher than those used in the SMFS measurements (*SI Appendix*), the stimulatory structure would be expected to pass through the force range most likely to induce conformational transitions multiple times, analogous to the conditions present in the SMFS measurements.

The results presented here suggest that it is primarily the dynamic properties of stimulatory structures, rather than their static properties, that are important for inducing −1 PRF. Pseudoknots are considered the canonical stimulatory structure and are often assumed to be the active element inducing −1 PRF (6, 21, 53, 54). Such an assumption seems unlikely to apply here, however: the prevalence of the pseudoknot structures PK_A, PK_D, and PK_D-, which combined were present only 34 ± 2% of the time at zero force, is insufficient to account for the −1 PRF efficiency of ~80% observed for this frameshift signal, even if each of the pseudoknot structures stimulated −1 PRF with 100% efficiency. Thus, some other factor(s) presumably must be involved. Indeed, the diversity of structures formed by the WNV frameshift signal at zero force raises the question of whether it is meaningful to speak of a single "native" structure stimulating frameshifting. We note that these considerations reflect the value of studying a frameshift signal with very high efficiency: it helps clarify the factors that must be important for stimulating −1 PRF.

The fact that the WNV frameshift signal—one of the highest-efficiency −1 PRF stimulators studied to date—exhibits the most complex, heterogeneous dynamics yet observed in any frameshift signal, along with the observation that the probability of structural transitions is most pronounced in the force range that the RNA is expected to experience during −1 PRF, suggest that the key factor for stimulating −1 PRF at high levels is most likely the propensity of the frameshift signal to undergo conformational changes when under tension from ribosomal attempts to translocate through it. We speculate that mechanistically, such conformational changes (whether near-equilibrium fluctuations or out-of-equilibrium switches) could trigger frameshifting by communicating abrupt tension fluctuations to the tRNA-mRNA complex, possibly in concert with other regulatory mechanisms yet to be fully elucidated. Such a picture is consistent with previous work connecting −1 PRF to pseudoknot conformational flexibility or dynamics (16, 18, 21, 30) and the ability to inhibit late-stage translocation during ribosome-induced unfolding of the first few base pairs (33). Notably, this perspective embeds the dynamic mechanical unfolding of the frameshift signal at the crux of the mechanisms that control −1 PRF efficiency. Future work extending single-molecule and kinetic assays of frameshifting (36, 55–57) to measure simultaneously the dynamics of both the ribosomal complex and the frameshift stimulatory structure in the act of frameshifting may help clarify the role of mRNA conformation dynamics in −1 PRF through more direct observation.

Methods

SMFS Measurements and Analysis. Samples were prepared, measured, and analyzed as reported previously (16) and described in detail in *SI Appendix*.

Dual-Luciferase Frameshift Assay. RNA transcripts were made containing the *Renilla* luciferase gene in the 0 frame upstream of the firefly luciferase in the −1 frame and separated by the WNV slippery sequence, linker, and stimulatory structure. Frameshifting efficiency was then measured from the luciferase luminescence ratio as described previously (58) and compared with values for negative and positive controls. Details are provided in *SI Appendix*.

ACKNOWLEDGMENTS. This work was supported by the Canadian Institutes of Health Research, the National Research Council Canada, and Alberta Innovates.

1. R. Ketteler, On programmed ribosomal frameshifting: The alternative proteomes. *Front. Genet.* **3**, 242 (2012).
2. I. Brierley, R. J. C. Gilbert, S. Pennell, "Pseudoknot-dependent programmed —1 ribosomal frameshifting: Structures, mechanisms and models" in *Recoding: Expansion of Decoding Rules Enriches Gene Expression, Nucleic Acids and Molecular Biology*, J. F. Atkins, R. F. Gesteland, Eds. (Springer, New York, 2010), pp. 149–174.
3. J. D. Dinman, Mechanisms and implications of programmed translational frameshifting. *Wiley Interdiscip. Rev. RNA* **3**, 661–673 (2012).
4. J. F. Atkins, G. Loughran, P. R. Bhatt, A. E. Firth, P. V. Baranov, Ribosomal frameshifting and transcriptional slippage: From genetic steganography and cryptography to adventitious use. *Nucleic Acids Res.* **44**, 7007–7078 (2016).
5. E. Dam, K. Pleij, D. Draper, Structural and functional aspects of RNA pseudoknots. *Biochemistry* **31**, 11665–11676 (1992).
6. D. P. Giedroc, P. V. Cornish, Frameshifting RNA pseudoknots: Structure and mechanism. *Virus Res.* **139**, 193–208 (2009).
7. E. P. Plant, "Ribosomal frameshift signals in viral genomes" in *Viral Genomes - Molecular Structure, Diversity, Gene Expression Mechanisms and Host-Virus Interactions*, M. L. Garcia, V. Romanowski, Eds. (Intech Open, 2012), pp. 93–122.
8. J. A. Kendra *et al*., Ablation of programmed −1 ribosomal frameshifting in Venezuelan equine encephalitis virus results in attenuated neuropathogenicity. *J. Virol.* **91**, e01766-e16 (2017).
9. E. B. Melian *et al*., Programmed ribosomal frameshift alters expression of West Nile virus genes and facilitates virus replication in birds and mosquitoes. *PLoS Pathog.* **10**, e1004447 (2014).
10. E. B. Melian *et al*., NS1′ of flaviviruses in the Japanese encephalitis virus serogroup is a product of ribosomal frameshifting and plays a role in viral neuroinvasiveness. *J. Virol.* **84**, 1641–1647 (2010).
11. I. Brierley, F. J. Dos Ramos, Programmed ribosomal frameshifting in HIV-1 and the SARS-CoV. *Virus Res.* **119**, 29–42 (2006).
12. D. Dulude, Y. A. Berchiche, K. Gendron, L. Brakier-Gingras, N. Heveker, Decreasing the frameshift efficiency translates into an equivalent reduction of the replication of the human immunodeficiency virus type 1. *Virology* **345**, 127–136 (2006).
13. M. Shehu-Xhilaga, S. M. Crowe, J. Mak, Maintenance of the Gag/Gag-Pol ratio is important for human immunodeficiency virus type 1 RNA dimerization and viral infectivity. *J. Virol.* **75**, 1834–1841 (2001).
14. A. T. Belew, J. D. Dinman, Cell cycle control (and more) by programmed -1 ribosomal frameshifting: Implications for disease and therapeutics. *Cell Cycle* **14**, 172–178 (2015).
15. P. C. Gareiss, B. L. Miller, Ribosomal frameshifting: An emerging drug target for HIV. *Curr. Opin. Investig. Drugs* **10**, 121–128 (2009).
16. D. B. Ritchie, D. A. Foster, M. T. Woodside, Programmed −1 frameshifting efficiency correlates with RNA pseudoknot conformational plasticity, not resistance to mechanical unfolding. *Proc. Natl. Acad. Sci. U.S.A.* **109**, 16167–16172 (2012).
17. S. Cao, S.-J. Chen, Predicting ribosomal frameshifting efficiency. *Phys. Biol.* **5**, 016002 (2008).
18. Y. Wang *et al*., Comparative studies of frameshifting and nonframeshifting RNA pseudoknots: A mutational and NMR investigation of pseudoknots derived from the bacteriophage T2 gene 32 mRNA and the retroviral gag-pro frameshift site. *RNA* **8**, 981–996 (2002).
19. P. V. Cornish, M. Hennig, D. P. Giedroc, A loop 2 cytidine-stem 1 minor groove interaction as a positive determinant for pseudoknot-stimulated −1 ribosomal frameshifting. *Proc. Natl. Acad. Sci. U.S.A.* **102**, 12694–12699 (2005).
20. E. P. Plant *et al*., A three-stemmed mRNA pseudoknot in the SARS coronavirus frameshift signal. *PLoS Biol.* **3**, e172 (2005).
21. C. Moomau, S. Musalgaonkar, Y. A. Khan, J. E. Jones, J. D. Dinman, Structural and functional characterization of programmed ribosomal frameshift signals in West Nile virus strains reveals high structural plasticity among cis-acting RNA elements. *J. Biol. Chem.* **291**, 15788–15795 (2016).
22. J.-D. Wen *et al*., Following translation by single ribosomes one codon at a time. *Nature* **452**, 598–603 (2008).
23. X. Qu *et al*., The ribosome uses two active mechanisms to unwind messenger RNA during translation. *Nature* **475**, 118–121 (2011).
24. T. M. Hansen, S. N. S. Reihani, L. B. Oddershede, M. A. Sørensen, Correlation between mechanical strength of messenger RNA pseudoknots and ribosomal frameshifting. *Proc. Natl. Acad. Sci. U.S.A.* **104**, 5830–5835 (2007).
25. O. Namy, S. J. Moran, D. I. Stuart, R. J. C. Gilbert, I. Brierley, A mechanical explanation of RNA pseudoknot function in programmed ribosomal frameshifting. *Nature* **441**, 244–247 (2006).
26. E. P. Plant *et al*., The 9-A solution: How mRNA pseudoknots promote efficient programmed −1 ribosomal frameshifting. *RNA* **9**, 168–174 (2003).
27. D. B. Ritchie, M. T. Woodside, Probing the structural dynamics of proteins and nucleic acids with optical tweezers. *Curr. Opin. Struct. Biol.* **34**, 43–51 (2015).
28. G. Chen, K.-Y. Chang, M.-Y. Chou, C. Bustamante, I. Tinoco, Jr, Triplex structures in an RNA pseudoknot enhance mechanical stability and increase efficiency of −1 ribosomal frameshifting. *Proc. Natl. Acad. Sci. U.S.A.* **106**, 12706–12711 (2009).
29. Z. Zhong *et al*., Mechanical unfolding kinetics of the SRV-1 gag-pro mRNA pseudoknot: Possible implications for −1 ribosomal frameshifting stimulation. *Sci. Rep.* **6**, 39549 (2016).
30. M. de Messieres *et al*., Single-molecule measurements of the CCR5 mRNA unfolding pathways. *Biophys. J.* **106**, 244–252 (2014).
31. D. B. Ritchie *et al*., Conformational dynamics of the frameshift stimulatory structure in HIV-1. *RNA* **23**, 1376–1384 (2017).
32. D. B. Ritchie, J. Soong, W. K. A. Sikkema, M. T. Woodside, Anti-frameshifting ligand reduces the conformational plasticity of the SARS virus pseudoknot. *J. Am. Chem. Soc.* **136**, 2196–2199 (2014).
33. B. Wu *et al*., Translocation kinetics and structural dynamics of ribosomes are modulated by the conformational plasticity of downstream pseudoknots. *Nucleic Acids Res.* **46**, 9736–9748 (2018).
34. M. M. Kuhlmann, M. Chattopadhyay, V. A. Stupina, F. Gao, A. E. Simon, An RNA element that facilitates programmed ribosomal readthrough in Turnip crinkle virus adopts multiple conformations. *J. Virol.* **90**, 8575–8591 (2016).
35. A. E. Firth, J. F. Atkins, A conserved predicted pseudoknot in the NS2A-encoding sequence of West Nile and Japanese encephalitis flaviviruses suggests NS1′ may derive from ribosomal frameshifting. *Virol. J.* **6**, 14 (2009).
36. S. Yan, J. D. Wen, C. Bustamante, I. Tinoco, Jr, Ribosome excursions during mRNA translocation mediate broad branching of frameshift pathways. *Cell* **160**, 870–881 (2015).
37. M. D. Wang, H. Yin, R. Landick, J. Gelles, S. M. Block, Stretching DNA with optical tweezers. *Biophys. J.* **72**, 1335–1346 (1997).
38. G. Chen, J.-D. Wen, I. Tinoco, Jr, Single-molecule mechanical unfolding and folding of a pseudoknot in human telomerase RNA. *RNA* **13**, 2175–2188 (2007).
39. J. Liphardt, B. Onoa, S. B. Smith, I. Tinoco, Jr, C. Bustamante, Reversible unfolding of single RNA molecules by mechanical force. *Science* **292**, 733–737 (2001).
40. M. T. Woodside *et al*., Nanomechanical measurements of the sequence-dependent folding landscapes of single nucleic acid hairpins. *Proc. Natl. Acad. Sci. U.S.A.* **103**, 6190–6195 (2006).
41. M. Zuker, Mfold web server for nucleic acid folding and hybridization prediction. *Nucleic Acids Res.* **31**, 3406–3415 (2003).
42. B. Onoa *et al*., Identifying kinetic barriers to mechanical unfolding of the T. thermophila ribozyme. *Science* **299**, 1892–1895 (2003).
43. K. Neupane, H. Yu, D. A. N. Foster, F. Wang, M. T. Woodside, Single-molecule force spectroscopy of the add adenine riboswitch relates folding to regulatory mechanism. *Nucleic Acids Res.* **39**, 7677–7687 (2011).
44. W. J. Greenleaf, K. L. Frieda, D. A. N. Foster, M. T. Woodside, S. M. Block, Direct observation of hierarchical folding in single riboswitch aptamers. *Science* **319**, 630–633 (2008).
45. S. Bellaousov, D. H. Mathews, ProbKnot: Fast prediction of RNA secondary structure including pseudoknots. *RNA* **16**, 1870–1880 (2010).
46. Y. Kato, K. Sato, K. Asai, T. Akutsu, Rtips: Fast and accurate tools for RNA 2D structure prediction using integer programming. *Nucleic Acids Res.* **40**, W29–W34 (2012).
47. S. Sen Mojumdar *et al*., Partially native intermediates mediate misfolding of SOD1 in single-molecule folding trajectories. *Nat. Commun.* **8**, 1881 (2017).
48. A. Solanki, K. Neupane, M. T. Woodside, Single-molecule force spectroscopy of rapidly fluctuating, marginally stable structures in the intrinsically disordered protein α-synuclein. *Phys. Rev. Lett.* **112**, 158103 (2014).
49. M. Chamorro, N. Parkin, H. E. Varmus, An RNA pseudoknot and an optimal heptameric shift site are required for highly efficient ribosomal frameshifting on a retroviral messenger RNA. *Proc. Natl. Acad. Sci. U.S.A.* **89**, 713–717 (1992).
50. J. Roca *et al*., Monovalent ions modulate the flux through multiple folding pathways of an RNA pseudoknot. *Proc. Natl. Acad. Sci. U.S.A.* **115**, E7313–E7322 (2018).
51. Y.-J. Wu, C.-H. Wu, A. Y.-C. Yeh, J.-D. Wen, Folding a stable RNA pseudoknot through rearrangement of two hairpin structures. *Nucleic Acids Res.* **42**, 4505–4515 (2014).
52. C. M. Kaiser, I. Tinoco, Jr, Probing the mechanisms of translation with force. *Chem. Rev.* **114**, 3266–3280 (2014).
53. X. Huang, Q. Cheng, Z. Du, A genome-wide analysis of RNA pseudoknots that stimulate efficient −1 ribosomal frameshifting or readthrough in animal viruses. *BioMed Res. Int.* **2013**, 984028 (2013).
54. B. Houck-Loomis *et al*., An equilibrium-dependent retroviral mRNA switch regulates translational recoding. *Nature* **480**, 561–564 (2011).
55. N. Caliskan, V. I. Katunin, R. Belardinelli, F. Peske, M. V. Rodnina, Programmed −1 frameshifting by kinetic partitioning during impeded translocation. *Cell* **157**, 1619–1631 (2014).
56. C. Chen *et al*., Dynamics of translation by single ribosomes through mRNA secondary structures. *Nat. Struct. Mol. Biol.* **20**, 582–588 (2013).
57. J. Chen *et al*., Dynamic pathways of −1 translational frameshifting. *Nature* **512**, 328–332 (2014).
58. G. Grentzmann, J. A. Ingram, P. J. Kelly, R. F. Gesteland, J. F. Atkins, A dual-luciferase reporter system for studying recoding signals. *RNA* **4**, 479–486 (1998).

PNAS
www.pnas.org

Supplementary Information for

Complex dynamics under tension in a high-efficiency frameshift stimulatory structure

Matthew T.J. Halma, Dustin B. Ritchie, Tonia R. Cappellano, Krishna Neupane, Michael T. Woodside

Corresponding author: Michael Woodside
Email: michael.woodside@ualberta.ca

This PDF file includes:

www.pnas.org/cgi/doi/10.1073/pnas.1905258116

SUPPLEMENTARY METHODS

RNA constructs for SMFS: DNA encoding the 111-nt NS1′ frameshift signal of the WNV New York strain located downstream of the 7-nt slippery sequence and 5-nt spacer region (accession number NC_009942, nucleotides 3558 to 3668, sequence listed in Table S1) was inserted into the pMLuc1 plasmid between the SpeI and BamHI restriction sites to produce a transcription template. The frameshift signal was flanked in the transcription template on both sides by 3-nt linkers. This transcription template was first amplified by PCR, including 840-nt and 2240-nt segments of the plasmid respectively upstream and downstream of the frameshift signal for use as handles in SMFS, then the PCR product was transcribed *in vitro* with T7 RNA polymerase. Two single-stranded DNA handles, complementary 3′ and 5′ ends of the transcript and labeled respectively with biotin and digoxigenin, were produced by asymmetric PCR from double-stranded DNA PCR products corresponding to the flanking handle sequences (1). These handles were annealed with the RNA transcript, then the product was incubated with 600-nm and 820-nm diameter polystyrene beads labeled respectively with avidin DN (Vector Labs) and antidigoxigenin (Roche) to create dumbbells for optical trapping measurements. Dumbbells were diluted to ~2 pM in measuring buffer (50 mM MOPS, pH 7.0, 130 mM KCl, 4 mM $MgCl_2$), 50 U/mL Superase•In RNase inhibitor (Ambion), and oxygen-scavenging system (40 U/mL glucose oxidase, 185 U/mL catalase, and 8.3 mg/mL glucose) and inserted into a sample chamber on a clean microscope slide in the optical trap. For experiments including anti-sense oligomers, 10 μM of the DNA oligo (Integrated DNA Technologies) was added to the measurement buffer.

SMFS measurements and analysis: FECs were measured using a custom-built dual-trap optical tweezers setup. The stiffness of the two traps were 0.58 and 0.37 pN/nm, calibrated as described previously (2). The traps were moved apart with acousto-optic deflectors at a constant speed of 200 nm/s to unfold the RNA, while the position of the beads was measured with position-sensitive diodes sampled at 20 kHz and filtered online at 10 kHz using an 8-pole Bessel filter. After unfolding, the traps were brought together at the same speed to refold the RNA, and the RNA was held at ~ 0 pN for 3 s before the next unfolding curve was initiated. The speed of the force ramps resulted in a loading rate of ~20–80 pN/s in the force range of 5–13 pN; in comparison, the loading rate applied by a ribosome during translocation can be estimated from the ~80-ms translocation time (3) and the stiffness of the 5–6-nt linker between the slippery sequence and the stimulatory structure as ~100–400 pN/s in the same force range.

FECs were modeled as two extensible worm-like chains in series, one for the duplex handles and the other for the unfolded RNA. Each WLC was fit to the function

$$F(x) = \frac{k_B T}{L_p}\left[\frac{1}{4}\left(1 - \frac{x}{L_c} + \frac{F}{K}\right)^{-2} - \frac{1}{4} + \frac{x}{L_c} - \frac{F}{K}\right], \qquad (1)$$

where L_p is the persistence length, L_c the contour length, and K the elastic modulus (4). The same handle parameters (L_c, L_p, and K) were used in the fits for all branches of the FECs measured from a given molecule, and the RNA parameters L_p = 1 nm, K ~ 1500 pN (5) were taken as fixed constants in all fits, so that the only parameter varying between branches was the contour length of unfolded RNA, L_c^U. After fitting, each portion of the

FEC was assigned to a structural state based on the fits to determine the trajectory of states followed. The transition map was then generated by combining the state trajectories from all FECs.

Dual-luciferase frameshift assay: The sequence corresponding to *Renilla* luciferase and the multiple cloning site from pMLuc1 was cloned into the pISO plasmid (Addgene) upstream of the firefly luciferase sequence in pISO, with the firefly luciferase in the −1 frame, creating a dual-luciferase reporting system. Three variants were produced: (i) the desired WNV construct, with slippery sequence (C CCC UUU), linker region (CAG UU), and 111-nt stimulatory structure sequence (Table S1) inserted between the two luciferases using the PstI and SpeI restriction sites; (ii) a negative control with a stop codon replacing part of the slippery sequence, to measure the background level of frameshifting-independent firefly luciferase expression; and (iii) a positive control without a slippery sequence and with in-frame *Renilla* and firefly luciferase open reading frames, to measure the maximum expected firefly:*Renilla* luciferase ratio. For each construct, the transcription template was amplified by PCR and the transcribed *in vitro* with T7 RNA polymerase.

Frameshifting efficiency was measured by dual-luciferase assay (6). Briefly, 2 µg of mRNA from each construct was heated to 65 ^{o}C, mixed with 35 µL of treated rabbit reticulocyte lysate (Promega) and 0.5 µL of 1 mM amino-acid mixture lacking Leu and Met, and then incubated for 90 min at 30 ^{o}C. Using a microplate reader (Turner Biosystems) to measure luminescence from each of the constructs, 20 µL of each reaction was incubated with 100 µL of Dual-Glo Luciferase reagent (Promega) in a well for 10 min, before quantifying firefly luminescence. Then 100 µL of Dual-Glo Stop and Glo reagent was added to each well to quench firefly luminescence, and *Renilla* luminescence was measured after 10-min incubation. The −1 PRF efficiency was then calculated from the ratio of firefly and *Renilla* luminescence, subtracting the background measured from the negative control and normalizing by the positive control. Four replicates were measured and the results averaged.

SUPPLEMENTARY REFERENCES

1. K. Neupane, H. Yu, D. A. N. Foster, F. Wang, M. T. Woodside, Single-molecule force spectroscopy of the add adenine riboswitch relates folding to regulatory mechanism. *Nucleic Acids Res*. **39**, 7677–7687 (2011).
2. K. C. Neuman, S. M. Block, Optical trapping. *Rev. Sci. Instrum.* **75**, 2787–2809 (2004).
3. J.-D. Wen et al., Following translation by single ribosomes one codon at a time. *Nature* **452**, 598–603 (2008).
4. M. D. Wang, H. Yin, R. Landick, J. Gelles, S. M. Block, Stretching DNA with optical tweezers. *Biophys. J*. **72**, 1335–1346 (1997).
5. Y. Seol, G. M. Skinner, K. Visscher, Elastic properties of a single-stranded charged homopolymeric ribonucleotide. *Phys. Rev. Lett.* **93**, 8–11 (2004).
6. G. Grentzmann, J. A. Ingram, P. J. Kelly, R. F. Gesteland, J. F. Atkins, A dual-luciferase reporter system for studying recoding signals. *RNA* **4**, 479–486 (1998).

Table S1: RNA and DNA sequences. Sequences of the WNV frameshift signal and anti-sense DNA oligomers.

WNV frameshift signal	5′- GGG CCU UCU GGU CGU GUU CUU GGC CAC CCA GGA GGU CCU UCG CAA GAG GUG GAC AGC CAA GAU CAG CAU GCC AGC UAU ACU GAU UGC UCU GCU AGU CCU GGU GUU UGG GGG -3′
Oligo 1	5′-CUUGGCUGUCC-3′
Oligo 2	5′-CCCCCAAACACCAGG-3′

Table S2: Average contour length of unfolded RNA and refolding forces observed for each conformational state. Errors represent s.e.m.

State	L_c^U (nm)	F_R (pN)
DHP	0	7.5 ± 0.1
DHP−	10 ± 1	8.2 ± 0.1
PK_D	11 ± 2	6.8 ± 0.2
PK_D−	14 ± 2	7.7 ± 0.2
PK_A+HP	20 ± 1	8.5 ± 0.1
PK_A	31 ± 1	9.9 ± 0.3
$S1_A$	39 ± 1	11.1 ± 0.2

Table S3: Unfolding lengths and forces in presence of anti-sense oligos. State PK_D−* is a version of PK_D− in which stem 2 is shortened by 2 nt owing to strand invasion by oligo 2. Errors represent s.e.m.

With oligo 1				
Observed state	**Observed L_c^U (nm)**	**Proposed state**	**Expected L_c^U (nm)**	**Observed F_U (pN)**
1	0	DHP	0	10±1
2	12 ± 1	$S1_A$-4	11.8	16±1
3	19.5 ± 0.4	$S1_A$-3	18.1	15.5±0.2
4	29 ± 1	$S1_A$-2	29.9	18.5±0.3
5	41.8 ± 0.5	$S1_A$	40.9	16.3±0.3
U	61.3 ± 0.2	U	61.3	

With oligo 2				
Observed state	**Observed L_c^U (nm)**	**Proposed state**	**Expected L_c^U (nm)**	**Observed F_U (pN)**
1	14.2 ± 0.3	PK_D−*	13.7	19±2
2	21 ± 1	PK_A+HP	20.5	12±1
3	31 ± 1	PK_A	31.5	23±1
4	42 ± 1	$S1_A$	40.9	17±1
U	61.3 ± 0.3	U	47.6	

Table S4: State occupancies at the start of unfolding FECs and the end of refolding FECs. The occupancies observed at the start of unfolding, average over all curves, were similar to the occupancies observed for the first unfolding curve from each individual molecule. Error bars represent s.e.m.

State	Unfolding (all curves)	Unfolding (first pulls)	Refolding (all curves)
DHP	0.16 ± 0.02	0.13 ± 0.08	0.19 ± 0.02
DHP−	0.50 ± 0.02	0.50 ± 0.1	0.29 ± 0.02
PK_D	0.13 ± 0.02	0.13 ± 0.08	0.12 ± 0.02
PK_D−	0.08 ± 0.01	0.06 ± 0.06	0.08 ± 0.01
PK_A+HP	0.09 ± 0.01	0.13 ± 0.08	0.20 ± 0.02
PK_A	0.04 ± 0.01	0.06 ± 0.06	0.10 ± 0.01
$S1_A$	0	0	0.02 ± 0.01

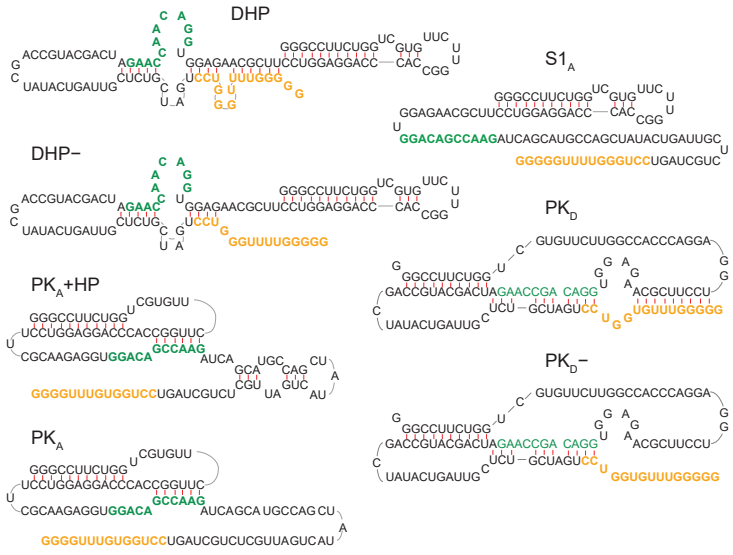

Figure S1: Secondary structure models of WNV frameshift signal conformations. Secondary structures are shown for each of the different conformations matching the states observed in the FECs, with base-pairing in red. The parts of the sequence complementary to anti-sense oligos 1 and 2 are indicated by green- and orange-colored bases, respectively.

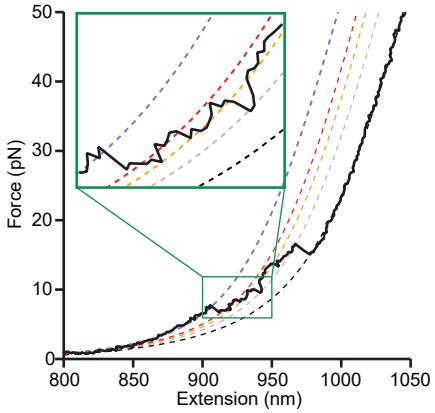

Figure S2: Reversible fluctuations between different conformations in FECs. Although FECs are inherently non-equilibrium measurements, some transitions were sufficiently close to equilibrium that reversible fluctuations between different structures could be observed. An example is shown here from an unfolding curve, with several examples of reversible 'hopping' between states highlighted in the inset. Dashed lines represent worm-like chain fits for DHP− (purple), PK_A+HP (red), PK_A (orange), $S1_A$ (grey), and unfolded (black).

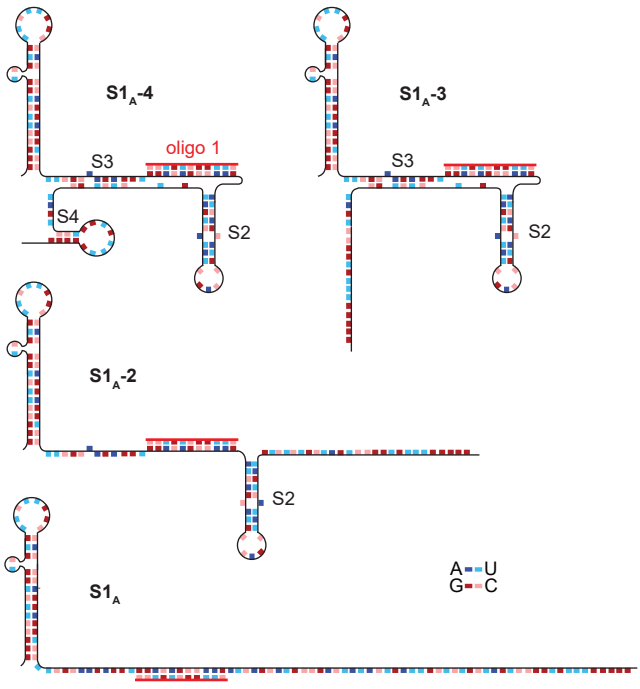

Figure S3: Secondary-structure models of states expected in the presence of oligo 1. One of the hairpins from the native folding ($S1_A$) remains, and three non-native helices (S2, S3, S4) can form.